

Article

Effects of Water-to-Cement Ratio on Pore Structure Evolution and Strength Development of Cement Slurry Based on HYMOSTRUC3D and Micro-CT

Shaojun Zheng ^{1,2}, Tianle Liu ^{1,2,*}, Guosheng Jiang ^{1,2}, Changliang Fang ^{1,2}, Bo Qu ¹ , Peng Gao ³ ,
Lixia Li ^{1,2} and Yingtao Feng ⁴

- ¹ Faculty of Engineering, China University of Geosciences, Wuhan 430074, China; sjzheng212@cug.edu.cn (S.Z.); jianggs@cug.edu.cn (G.J.); fangcl@cug.edu.cn (C.F.); qubooil@gmail.com (B.Q.); llx1039304620@cug.edu.cn (L.L.)
- ² Unconventional Cementing and Special Reinforcement Laboratory, China University of Geosciences, Wuhan 430074, China
- ³ School of Materials Science and Engineering, South China University of Technology, Guangzhou 510640, China; gaop@scut.edu.cn
- ⁴ Oilfield Chemistry Research and Development Institute, COSL, Sanhe 065201, China; fengyt@cosl.com.cn
- * Correspondence: liutianle2008@163.com; Tel.: +86-457-1532-718-5363

Abstract: Changing the water-to-cement ratio is one of the major ways to develop cement slurry with different densities, which in turn will greatly affect the pore structure and mechanical properties of cement slurry. In the current study, the cement hydration model HYMOSTRUC3D was used to investigate the effects of water-to-cement (w/c) ratio (0.40, 0.44, 0.50) on the pore structure evolution and strength development of cement slurry. The microstructure of the cement stone was characterized via scanning electron microscope (SEM) and micro-computed tomography (micro-CT), and the mechanical strength of the cement stone was tested and analyzed via a mechanical tester. The simulated compressive strength and capillary porosity are in good agreement with the measured data, where the relative error between the simulated results and measured results are within 0.6–10.7% and 13.04–25.31%, respectively. The capillary porosity is proved as the main factor affecting the compressive strength of cement stone with different w/c ratios. Herein, the mathematical relationship between the measured capillary porosity and compressive strength could be well fitted via the mathematical prediction models of the Balshin function ($R^2 = 0.95$), Ryshkewitch function ($R^2 = 0.94$), Schiller function ($R^2 = 0.96$), and the linear regression function ($R^2 = 0.95$). Moreover, the linear regression function ($y = -2.38x + 82.76$) can be used to characterize and predict the quantitative relationship between the compressive strength and capillary porosity of cement stone. The findings in this study will provide a reference value in the fields of oil and gas cementing and building concrete.

Keywords: hydration model; cement slurry; microstructure; w/c ratio; compressive strength; capillary porosity



Citation: Zheng, S.; Liu, T.; Jiang, G.; Fang, C.; Qu, B.; Gao, P.; Li, L.; Feng, Y. Effects of Water-to-Cement Ratio on Pore Structure Evolution and Strength Development of Cement Slurry Based on HYMOSTRUC3D and Micro-CT. *Appl. Sci.* **2021**, *11*, 3063. <https://doi.org/10.3390/app11073063>

Academic Editor: Doo-Yeol Yoo

Received: 2 March 2021

Accepted: 26 March 2021

Published: 30 March 2021

Publisher's Note: MDPI stays neutral with regard to jurisdictional claims in published maps and institutional affiliations.



Copyright: © 2021 by the authors. Licensee MDPI, Basel, Switzerland. This article is an open access article distributed under the terms and conditions of the Creative Commons Attribution (CC BY) license (<https://creativecommons.org/licenses/by/4.0/>).

1. Introduction

Cement slurry is typically utilized in filling the annular space between the pipe and rock formation, sealing casing columns, preventing formation series collusion, protecting production reservoirs, and stabilizing the oil and gas wells [1–6]. In the duration of the lifetime of oil and gas wells, they are prone to leakage at any time after the commencement of production [7], which may bring many problems to both field production and the ecological environment [8]. Due to the particularity of oil and gas well cementing engineering, a variety of cementing slurry systems with different density ranges are often used in the cementing process and changing the w/c ratio is one of the main and effective ways to develop cementing slurry with different densities. It is worth noting that the workability and durability of the cement sheath are strongly affected by the w/c ratios [9]. Meanwhile,

the w/c ratios greatly affect the pore structure and mechanical properties of cement slurry, in which case the porosity and mechanical properties are the main parameters to characterize the durability and service life of the cement sheath.

Over the past decades, many researchers [10–13] investigated the influence of the w/c ratio and curing age on the pore structure evolution and mechanical properties of cementitious materials. Schulze [10] illustrated that the influence of w/c and cement content on the properties of polymer-modified mortars has a similar influence as unmodified mortars. The compressive strength decreased with increasing w/c ratio and the cement content was of minor influence, while shrinkage and water absorption increased with the water–cement ratio and cement content. Rahmani et al. [12] demonstrated that the abrasion resistance of concrete is improved by 42% and the porosity of concrete is decreased to 13.1% by reducing the w/c ratio from 0.46 to 0.30 in nano-silica concrete specimens. Li et al. [13] used ice particles instead of liquid water as mixing water to prepare cement pastes and found that the total porosity is the main factor in determining the compressive strength of hardened cement paste with super low w/c ratios.

Furthermore, based on different experimentally measured results [14–18], different types of mathematical prediction models and regression models have focused on the relationship between porosity and strength. Anya et al. [19] derived an empirical model to calculate the uniaxial compressive strength of cement stone and studied the relationship between ultrasonic pulse transit time, density, w/c ratio, water-solids ratio, and strength. Wei et al. [20] discussed the pore volume fractal dimension of low-density microsphere cement and its relationship with pore structure and mechanical properties. Li et al. [13] established the relationship between compressive strength and total porosity of hardened cement paste with super low w/c ratios according to the Balshin function, Ryshkewitch function, and Schiller function. The relationship between the strength of hardened cement paste and the w/c ratio is well-studied. However, there are few reports on how the compressive strength of cement slurry is produced and what its influencing factors are. In addition, the study concentrated on cement slurry about the relationship between capillary porosity and compressive strength under different w/c ratios is not clear.

Recently, micro-CT has become a popular technique widely used in evaluating the microstructure property of cementitious materials due to its simple and non-destructive characteristics and short test time. Eric et al. [21] began to study the internal damage characteristics of Portland cement hydration products based on micro-CT in 1997 and found that the research and application of micro-CT in the field of cement concrete has increased dramatically. Micro-CT was initially used to investigate the internal structure of cement such as pore types (pores and damages) [22], pore shapes [23–26], and pore network [27,28]. The statistical and morphological analyses based on micro-CT provide a new view of the cement microstructure because they can provide a realistic 3D geometry [29].

With rapid computer technology developing, numerical approaches have drawn great attention from lots of scholars. Many kinds of cement hydration models have been established gradually, such as the Jennings-Johnson model [30], HYMOSTRUC3D model [31–33], Navi-Pignat model [34], CEMHYD3D model [35], DuCOM model [36], μ c model [37], HydratiCA model [38], THAMES model [39], Park's model [40], Thermodynamic modeling [41], etc. The above hydration models provide a new solution for the study on microstructure evolution and hydration mechanism of cement-based materials. In this paper, the HYMOSTRUC3D model was selected to simulate the hydration process and the microstructure development of cement slurry. Instead of using a certain characteristic particle size to represent its real particle size distribution, the HYMOSTRUC3D model [31–33] can consider the continuous particle size distribution of cement particles. The HYMOSTRUC3D model is a function of the clinker composition, particle size distribution of cement, w/c ratios of cement paste, and temperature in which the hydration of cement particle is controlled by the strict stereological principle and chemical reaction kinetics principle. The three-dimensional structure of cement slurry can be reconstructed, and the dynamic hydration process of cement slurry can be displayed with the visualiza-

tion software Para View. Compared with other hydration models, the HYMOSTRUC3D model is more rigorous and powerful. The model was first proposed to calculate the hydration rate of cement particles, during which the hydration process was divided into two stages (phase boundary reaction stage and diffusion-controlled reaction stage) based on the hydration rate parameters k_0 and δ_{tr} . Since then, the HYMOSTRUC3D model has been developed dramatically. Up to now, the HYMOSTRUC3D model has been used to simulate many properties of cement-based materials and blended cement-based materials, including the mechanical properties [31,42], microstructure [32], the autogenous shrinkage [33], the transport properties [43], the tensile strength and stiffness [44] of cement-based materials.

Hence, the HYMOSTRUC3D and micro-CT models were selected to study the effects of the w/c ratio on pore structure evolution and strength development of cement slurry. The relationships between cement clinker, hydration products, porosity, compressive strength, etc. with w/c ratios (0.40, 0.44, 0.50) and hydration times (1, 3, 7, 28, 140 days) were obtained from the cement slurry hydration kinetics model established on the HYMOSTRUC3D model [33], and the simulated results were compared with the measured results (mechanical tester and micro-CT). Moreover, the relationship between the compressive strength and capillary porosity was established by the mathematical prediction models (Balshin function, Ryshkewitch function, Schiller function [45,46], and linear function), and the residuals of those mathematical models were analyzed. The evolution mechanisms of pore structure were discussed via SEM. The findings of this study have certain application prospects in the fields of oil and gas cementing and building concrete.

2. Materials and Methods

The flowchart of the research approach is shown in Figure 1. The cement hydration model HYMOSTRUC3D, the experimental analysis methods (mechanical tester, micro-CT, and SEM), the mathematical prediction models (Balshin function, Ryshkewitch function, Schiller function [45,46] and linear function) were combined to study the effects of the w/c ratio on the pore structure evolution and strength development of cement slurry. Moreover, the residuals of those mathematical models were analyzed, and the evolution mechanisms of pore structure were discussed.

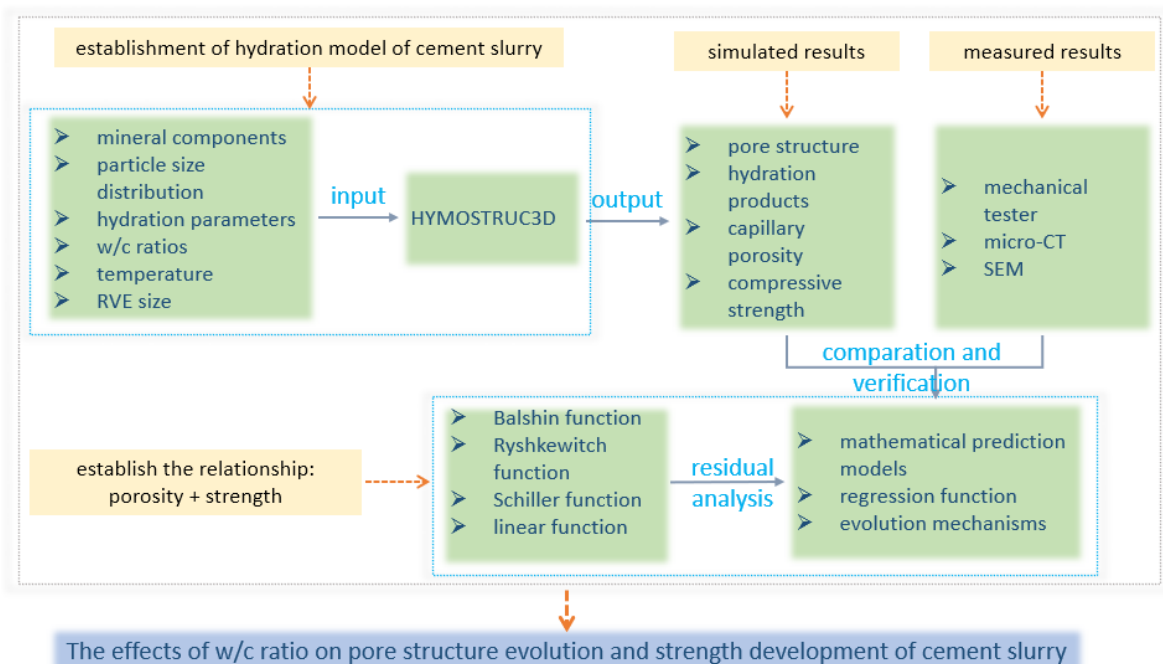


Figure 1. The flowchart of the research approach.

2.1. Materials

High sulfate-resistant grade G oil-well cement (GOC, according to Chinese National Standard GB/T 10238-2015, manufactured in Shandong Special Cement Co., Ltd., Shandong, China) with a density of 3.15 g/cm^3 was used to make the slurries, and the mineral components of the GOC are listed in Table 1. The particle size distribution of the GOC was tested by a laser diffraction particle size analyzer (Mastersizer 3000, Malvern Panalytical, UK), and the cumulative volume fraction of cement particles was fitted by the Rosin–Rammler–Bennet (RRB) function ($y = 100 - 100\exp(-bx^n)$, where y is the cumulative volume fraction, x is the particle size of the GOC, b and n are fitting parameters). The RRB function ($y = 100 - 100\exp(-0.04143x^{1.02})$) can be used to represent the distribution of cement particles. The results are shown in Figure 2.

Table 1. The mineral components of GOC.

Phase	C ₃ S	C ₂ S	C ₃ A	C ₄ AF	CSH ₂
Mass fraction/%	63.49	13.26	2.00	15.81	4.08

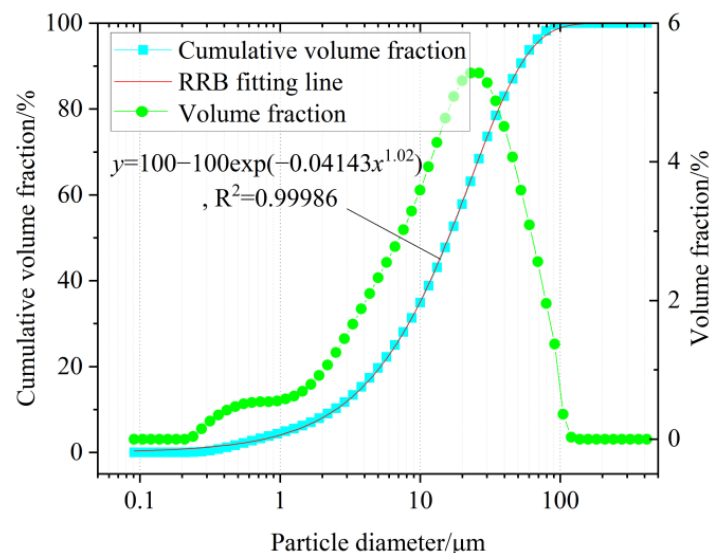


Figure 2. Particle size distribution of GOC.

In order to eliminate aeration, a transparent defoamer with a PH of 7.0 ± 0.5 and a density of $1.00 \text{ g/cm}^3 \pm 0.02 \text{ g/cm}^3$ was used. The defoamer is a mixture of refined hydrocarbons and unsaturated fatty acid esters. The slurry also contained a light-yellow antifiltrating agent with a PH of 5.5 ± 0.5 and a density of $1.08 \text{ g/cm}^3 \pm 0.01 \text{ g/cm}^3$. The antifiltrating agent is composed of AMPS Copolymer. All the above agents were supplied by Oilfield Chemistry Research Institute of CNOOC Oilfield Services Co., Ltd., Hong Kong, China. The slurry was prepared according to the Chinese National Standards GB/T 10238-2015. Three different w/c ratios of 0.40, 0.44, and 0.50 were selected in this work. The composition of the prepared cement slurry is summarized in Table 2. After mixing, the fresh cement slurry was cast into steel molds ($50.8 \text{ mm} \times 50.8 \text{ mm} \times 50.8 \text{ mm}$ for the compressive strength test, and $\phi 25 \text{ mm} \times 100 \text{ mm}$ for the micro-CT test) and pre-cured in a water bath at a temperature of $30 \text{ }^\circ\text{C}$.

Table 2. Selected compositions of cement slurries.

Composition	Action	1	2	3
w/c ratio		0.40	0.44	0.50
defoaming agent	eliminate aeration	0.5	0.5	0.5
antifiltrating agent	reduce cement slurry filtration	6	6	6
GOC	sets the cement slurry	100	100	100

All components in % by mass of cement.

2.2. Experimental Analysis Methods

2.2.1. Compressive Strength Analysis

The values of the compressive strength of the experimental samples were measured using a mechanical tester (ZCYA-W300C, Jinan Xinghuo testing machine Co., Ltd., Jinan, China). For each group, six cubical samples (50.8 mm × 50.8 mm × 50.8 mm) were tested and then the average of the compressive strength of each group was used as the final test result to ensure the accuracy of the test results.

The simulated compressive strength was calculated through the HYMOSTRUC3D model. Sun et al. [47,48] concluded that the effective contact area (A_{EC}) between particles is the main parameter to determine the bearing capacity of a cementitious material. In the HYMOSTRUC3D model, A_{EC} is defined as the contact area in the direction normal to the direction of the applied load. Taking the load applied in the y direction as an example, the particle contact relationship can be divided into four cases, as shown in Figure 3. A_{EC-y} is the sum of the effective contact area of all particles in the representative element volume (REV) in the y direction, $A_{EC-y} = \sum_{i=1}^n A_{EC-y,i}$. The total effective contact area A_{EC} is defined as the average value of A_{EC} in x, y, and z directions, that is, $A_{EC} = (A_{EC-x} + A_{EC-y} + A_{EC-z})/3$.

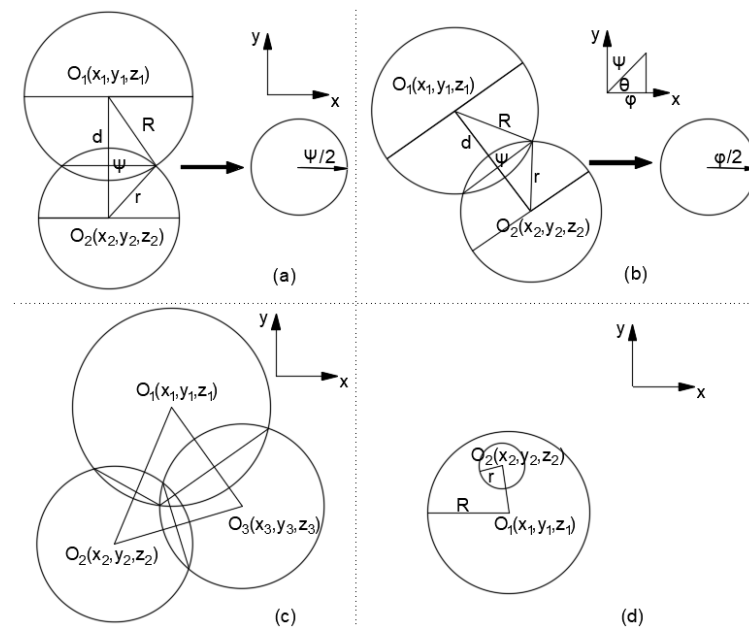


Figure 3. Effective contact area between different cement particles, modified from references [47,48]: (a) two particles interconnected in a plane perpendicular to the y-axis; (b) two particles not interconnected in a plane perpendicular to the y-axis; (c) three or more particles interconnected; (d) the larger particle O_1 contained the smaller particle O_2 completely.

2.2.2. Fractured Surface Morphology

The morphology of the samples was observed by SEM (Phenom™ XL G2, Eindhoven, Phenom Scientific, Eindhoven, The Netherlands).

2.2.3. Pore Structure Analysis

In this study, a micro-CT instrument (nano voxel-3000, Tianjin Sanying Precision Instrument Co., Ltd., Tianjin, China, as shown in Figure 4) was chosen to scan the samples. The X-ray energy of this micro-CT was 150 kV/60 mA, and a high-resolution microscopy detector was used with a pixel density of 2048×2048 and a resolution of $2 \mu\text{m}$. The sample was scanned from 0° to 360° with two scans per degree, and the exposure time for each scan was 1 s. The data matrix of X-ray intensities and radiographs was collected by the CCD detector. Moreover, the Voxel Studio Recon software was used to reconstruct the 3D microstructure, the Avizo Fire 8 [49,50] was used to perform the image segmentation of the samples with a measured resolution of $3.38 \mu\text{m}$ and a grayscale range of 0–65,535 (i.e., $2^{16}-1$).



Figure 4. Picture of nano voxel-3000.

Due to the limitations of calculation time and workstation configuration, it is difficult to perform calculations for the whole 3D reconstructed image [51]. A common approach is to select a volume of interest (VOI) [52]. Yio et al. [53] suggested that the physical length of the VOI should be bigger than $100 \mu\text{m}$. Fuisseis et al. [51] proposed that $200 \times 200 \times 200$ voxels should be a practical limit for supervised algorithms. Liu et al. [52] also determined that $200 \times 200 \times 200$ voxels were sufficient to represent the structure of the sample. Therefore, $200 \times 200 \times 200$ voxels were selected as the VOI.

In the 3D reconstructed image, according to their respective gray values, the phases can be segmented to determine their spatial positions and volumes. Based on the global threshold method [51,53,54], the threshold segmentation of pores was carried out to reconstruct the pore structure of the cement paste. To analyze the pore structure and capillary porosity, three VOIs were intercepted for each analysis of capillary porosity, and the average value was used as the final test result. The specific analysis process is shown in Figure 5.

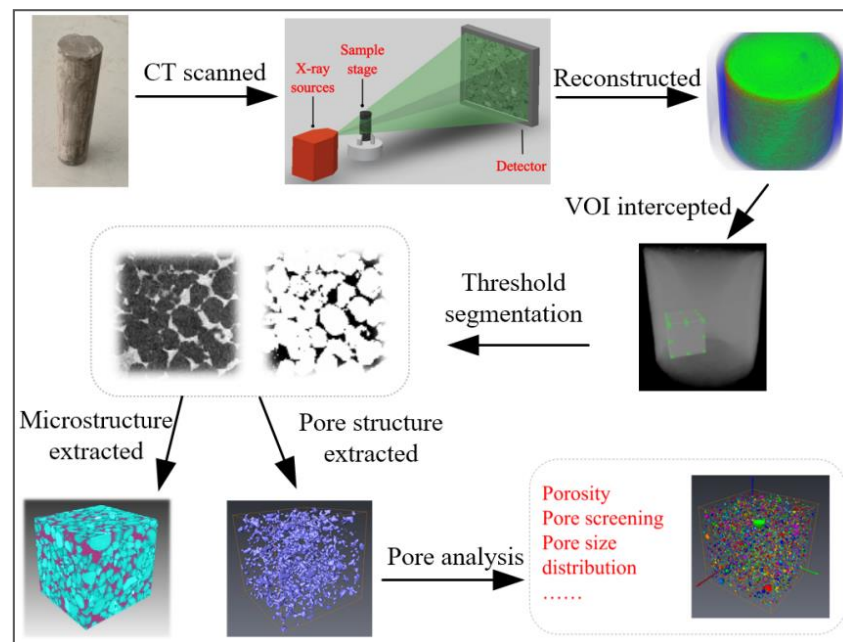


Figure 5. The flowchart of pore structure test and analysis using micro-CT.

2.3. Establishment of Hydration Kinetics Model of Cement Slurry with HYMOSTRUC3D

Wang et al. [55–57] demonstrated that mineral components can affect the initial hydration rate of cement paste dramatically. Referring to the research results of Nguyen et al. [56,57], the hydration parameters K_0 and δ_{tr} of GOC were calculated to be $0.0503 \mu\text{m}/\text{h}$ and $2.35 \mu\text{m}/\text{h}$, respectively, as shown in Table 3.

Table 3. The hydration parameters of GOC.

Phase		C_3S	C_2S	C_3A	C_4AF	GOC
Hydration parameters	K_0 ($\mu\text{m}/\text{h}$)	0.0713	0.0047	0.0644	0.02	0.0503
	δ_{tr} ($\mu\text{m}/\text{h}$)	2.66	3.07	3.58	1.19	2.35

Zhang et al. [58] suggested that the REV size of cementitious materials selected for HYMOSTRUC3D simulation should be $100^3 \mu\text{m}^3$. However, some cement particles are larger than $100 \mu\text{m}$ in diameter (as shown in Figure 1), thus, $REV = 200 \mu\text{m}$ was selected.

Then, hydration coefficients such as the particle size distribution (RRB fitting results), cement mineral composition, hydration parameters of cement, the w/c ratio, and REV size were substituted into the HYMOSTRUC3D model to establish the cement slurry hydration model, and the compressive strength, porosity, and hydration products of the cement slurry were obtained.

3. Results and Discussion

3.1. Compressive Strength

Figure 6 presents the simulated and measured compressive strength of cement samples at hydration times of 1, 3, 7, 28, and 140 days, in which the error bar represents the standard deviation. As can be seen from Figure 6, the compressive strength of the cement stone decreased with the increasing w/c ratio from 0.40 to 0.50 and increased with the increasing hydration time at the same w/c ratio.

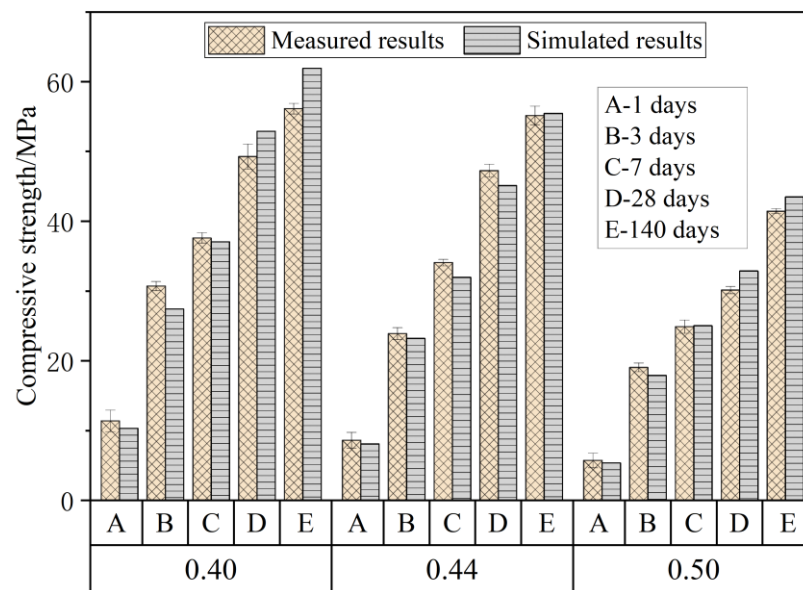


Figure 6. Measured and simulated compressive strength of cement stone.

With the increase of w/c ratio from 0.40 to 0.44, the compressive strength of the cement stone at 1, 3, 7, 28, and 140 days decreased by 24.30%, 22.17%, 9.41%, 4.12%, and 1.75%, respectively. With the increase of the w/c ratio from 0.44 to 0.50, the compressive strength of the cement stone at 1, 3, 7, 28, and 140 days decreased by 33.49%, 20.24%, 26.94%, 36.22%, and 24.86%, respectively. When the w/c ratio was 0.40, the daily growth rates of compressive strength of the cement paste from 1 to 3 days, 1 to 7 days, 1 to 28 days, and 1 to 140 days were 84.74%, 38.33%, 12.31%, and 2.82%, respectively, and the daily growth rate of compressive strength markedly decreased with the hydration time.

It also can be seen from Figure 6 that, when the w/c ratio is 0.40, 0.44, and 0.50, respectively, the relative deviation between the simulated results and measured results is 1.5~10.7%, 0.5~9.2%, and 0.6~9.1%, respectively. The maximum relative deviation between the simulated results and measured results is 10.7%, which indicates that the simulated results are in good agreement with the measured results.

3.2. Capillary Porosity

Figure 7 shows the capillary porosity gotten from the micro-CT and HYMOSTRUC3D models, in which the error bar represents standard deviation. As Figure 7 indicates, the capillary porosity of the cement stone increased with the increase in the w/c ratio and decreased with the increase in hydration time. With the increase of the w/c ratio from 0.40 to 0.44, the capillary porosity of cement stone at 1, 3, 7, and 28 days increased by 6.85%, 11.39%, 6.64%, and 23.07%, respectively. With the increase of the w/c ratio from 0.44 to 0.50, the capillary porosity of the cement stone at 1, 3, 7, and 28 days increased by 3.08%, 6.94%, 10.59%, and 12.81%, respectively.

When the w/c ratio was 0.40, the daily reduction rates of capillary porosity of the cement slurry from 1 to 3 days, 1 to 7 days, and 1 to 28 days were 13.62%, 6.02%, and 1.91%, respectively. The daily reduction rate of capillary porosity markedly decreased with the hydration time, while the decreasing trend reduced dramatically. In addition, the porosity of cement stone increased with the increase in the w/c ratio, which is contrary to the changing trend of compressive strength.

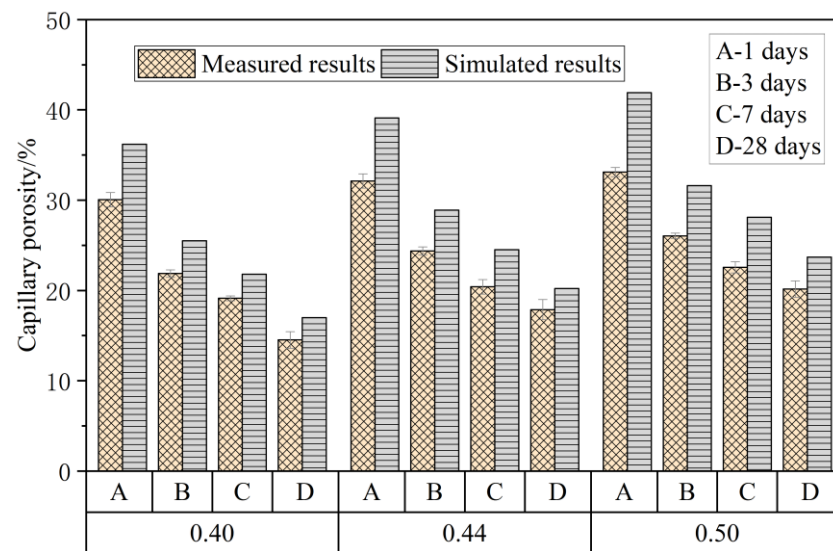


Figure 7. Measured and simulated capillary porosity of cement stone.

The relative deviations between the simulated results and measured results were 13.95~20.43%, 13.04~21.73%, and 17.56~25.31%, while the water–cement ratios were 0.40, 0.44, and 0.50, respectively.

It can be seen from Figures 6 and 7 that the capillary porosity increased with the increase in the w/c ratio at the same hydration time, while the mechanical strength decreased as the w/c ratio increased. In the well cementing industry, a lower w/c ratio should be selected as far as possible to prepare cement slurry and thus improve the early mechanical properties of the cement sheath.

Comparing the porosity results gotten from the micro-CT and HYMOSTRUC3D models, the micro-CT-measured results were smaller than those of the HYMOSTRUC3D model, while the overall trend of the porosity measured by the micro-CT model is consistent with the porosity simulated by the HYMOSTRUC3D model. The analysis shows that the resolution of the HYMOSTRUC3D model is 1 μm , while the resolution of the micro-CT model is 3.38 μm . Therefore, the measured porosity is lower than the simulated porosity, which can be attributed to CT not recognizing the pores between 1 and 3.38 μm . The limited resolution of the micro-CT model is the main reason for the smaller porosity values compared with the HYMOSTRUC3D simulated results, micro-CT is inadequate for testing nanoscale and sub-micron pores.

However, as Liu et al. [49] concluded, it is very important to obtain pore structures with large volumes in the cement stone. Silva et al. [59] also demonstrated that the big capillary pores can be correlated to the strength properties of the cement paste. Hence, the following discussion in Section 3.4 is based on the measured results, in which the influence of capillary porosity (pores larger than 3.38 μm in diameter) on the compressive strength of cement stone is discussed.

3.3. Pore Structure Evolution

The changes in volume fraction of mineral components and hydration products were evaluated by the HYMOSTRUC3D model, the results were shown in Figure 8. As shown in Figure 9, the 3D microstructures of the cement stone with the w/c ratio of 0.44 at 0, 1, and 28 days were reconstructed by the Para View visualization software.

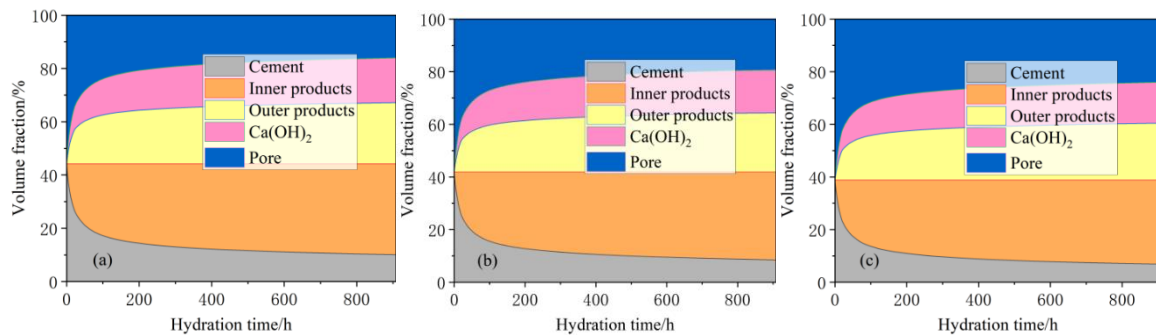


Figure 8. Time-varying curves of volume fraction of mineral components and hydration products under different w/c ratios using HYMOSTRUC3D. (a) 0.40; (b) 0.44; (c) 0.50.

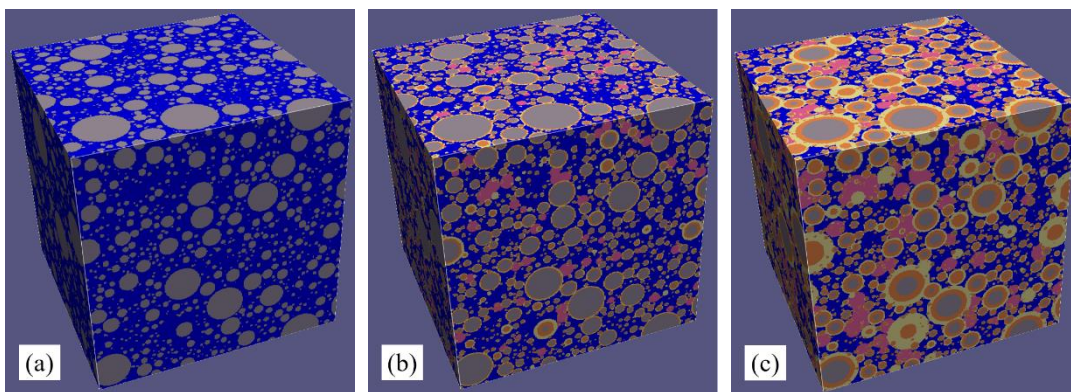


Figure 9. Microstructure of cement stone under different hydration time using HYMOSTRUC3D (a) 0 days; (b) 1 day; (c) 28 days.

At the initial hydration stage, the volume content of pores accounts for a relatively higher proportion than those at the later hydration stage. The pores are mostly connected pores and occupied by water (Figures 8 and 9a). As the hydration reaction proceeded and the degree of hydration increased, unhydrated cement particles and water decreased sharply. Lots of hydration products such as C-S-H gel and CH were generated gradually, resulting in a volumetric expansion effect, and they occupied the pore spaces (Figures 8 and 9). The lower capillary porosities indicated that the pores were filled with continuously formed hydration products [60]. As a result, the microstructures become more compact with the increase in hydration time at the same w/c ratio (Figure 9).

With the further hydration of cement, hydration products were continuously generated and wrapped onto the surface of unhydrated cement (Figure 9b,c). Meanwhile, the hydration products continuously formed and hindered the migration of water and ions, resulting in the hydration rate of GOC gradually slowing down, the isolation of pores, and the gradual optimization of pore structure. At the later hydration stage, capillary water was almost consumed absolutely, finally forcing the hydration reaction to stop. Meanwhile, the skeleton of cement slurry was basically constructed, and almost all pores were no longer connected [61].

Capillary pores are commonly considered the remnants of the initially water-filled space [62,63]. With the w/c ratio increasing from 0.40 to 0.44 and 0.44 to 0.50, the initial water volume ratio increased by 2.34% and 3.09% respectively. Correspondingly, the pore spaces and the capillary porosity increased with the increase in the w/c ratio at the same hydration time (Figure 10). On the contrary, the mechanical strength decreased as the w/c ratio increased.

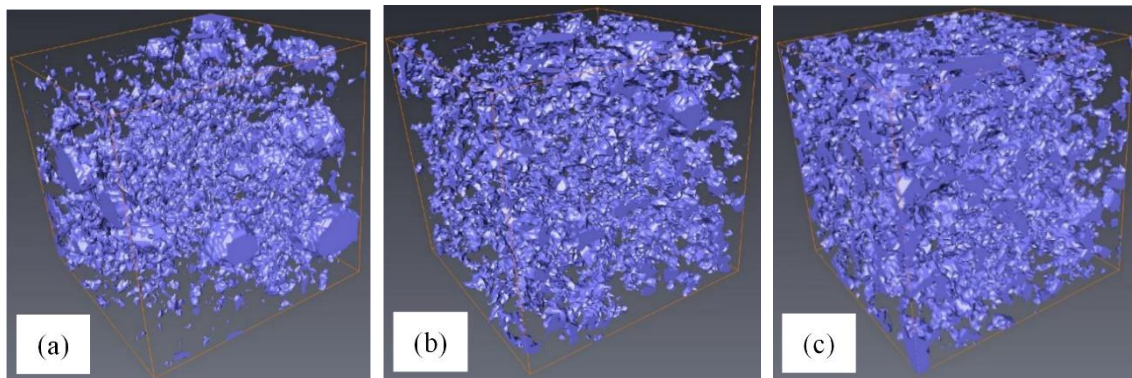


Figure 10. Pore structure of cement stone at 28 days under different w/c ratios using micro-CT (a) 0.40; (b) 0.44; (c) 0.50.

3.4. The Relationship between Compressive Strength and Capillary Porosity

Based on the analysis in Figures 6–10, the capillary porosities of the cement stone increased and the compressive strengths decreased with the increase in the w/c ratio at the same hydration time. The compressive strength and the capillary porosity of the cement stone were negatively correlated. To present the relationship between compressive strength and porosity of the cement stone, three widely accepted functions, the Balshin function, Ryshkewitch function, and Schiller function [45,46] were chosen and described as follows:

Balshin function,

$$y = a(1 - x/100)^b \quad (1)$$

Ryshkewitch function,

$$y = ae^{-bx} \quad (2)$$

Schiller function,

$$y = a \ln(b/x) \quad (3)$$

One linear function,

$$y = ax + b \quad (4)$$

where, y is the compressive strength of the cement stone, MPa; x is the capillary porosity of the cement stone, in percentage; a and b are fitting parameters.

In this study, the Balshin function, Ryshkewitch function, and Schiller function were used to fit the relationship between compressive strength and porosity, and the results are shown in Figure 11. According to the analysis in Figure 11, the correlation coefficients (R) between the measured compressive strength and the predicted results of Balshin function, Ryshkewitch function, and Schiller function were no less than 0.970 (i.e., $R^2 \geq 0.94$) (Figure 11a–c), which indicated that the correlation between compressive strength and the porosity of cement paste is high. A linear function was used to fit the relationship between compressive strength and porosity. The result is plotted in Figure 11d, and the correlation coefficient was 0.975 (i.e., $R^2 \geq 0.95$). Furthermore, the accuracy of the model function in predicting compressive strength was estimated based on statistical analysis. The predicted results were compared with the measured results (Table 4). Except for individual abnormal data points, the internally studentized residuals of the prediction model were all within the range of $[-2, 2]$. The individual abnormal data points within the range of $(-\infty, -2) \cup (2, \infty)$ of the internal studentized residuals were judged as abnormal points at the 95% confidence level, which was ignored in the regression straight line fitting. Hence, the occurrence of abnormal points will not affect the fitting results. It can also be found from Table 3 that there were no abnormal points in the fitting results of the one linear function, which indicates that $y = -2.38x + 82.76$ was the most representative function. It proved that the relationship between the compressive strength and porosity could be established by the linear function. Combining the results in Figure 10 with Section 3.2, the

capillary porosity is the main factor in determining the compressive strength of the cement stone, which is consistent with the result of Pandey et al. [16,45,46].

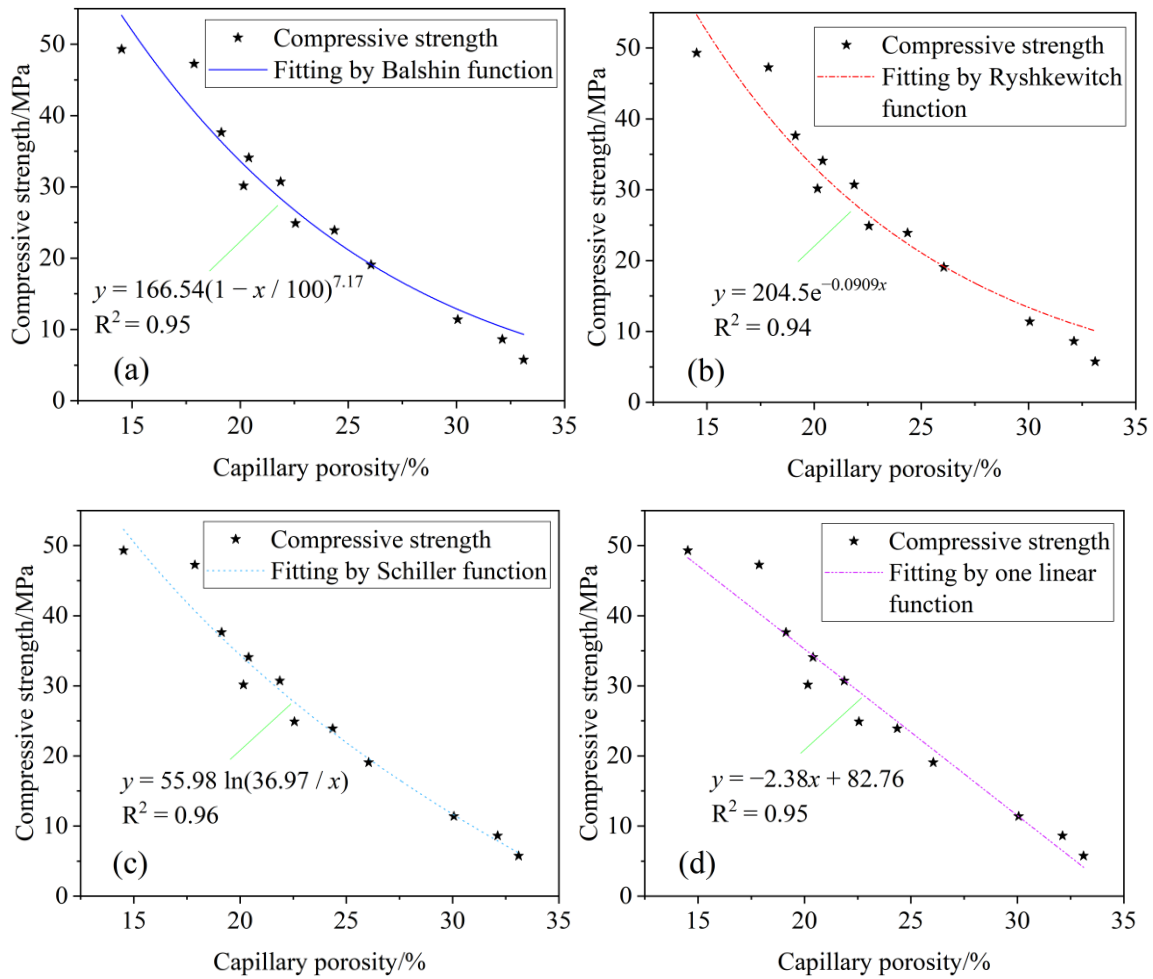


Figure 11. The relationship between compressive strength and capillary porosity of a cement stone. (a) Fitting by Balshin function; (b) Fitting by Ryshkewitch function; (c) Fitting by Schiller function; (d) Fitting by one linear function.

Table 4. Statistical analysis results of prediction functions of compressive strength.

Function	Measured Results	Predicted Results	Residual	Internally Studentized Residuals
Balshin function	49.30	54.07	−4.77	2.093
	47.27	40.60	6.67	−1.714
	37.62	36.34	1.28	−0.209
	30.15	33.15	−3.00	0.992
	34.08	32.44	1.64	−0.423
	30.72	28.38	2.34	−0.744
	24.90	26.63	−1.73	0.432
	23.91	22.50	1.41	−0.624
	19.07	19.13	−0.06	−0.274
	11.40	12.83	−1.43	−0.033
	8.63	10.35	−1.72	−0.013
	5.74	9.32	−3.58	0.518
	49.30	54.64	−5.34	2.233

Table 4. Cont.

Function	Measured Results	Predicted Results	Residual	Internally Studentized Residuals
Ryshkewitch function	47.27	40.29	6.98	−1.579
	37.62	35.93	1.69	−0.264
	30.15	32.72	−2.57	0.805
	34.08	32.02	2.06	−0.485
	30.72	28.01	2.71	−0.785
	24.90	26.31	−1.41	0.291
	23.91	22.34	1.57	−0.646
	19.07	19.16	−0.09	−0.289
	11.40	13.30	−1.90	0.027
	8.63	11.03	−2.40	0.095
	5.74	10.08	−4.34	0.597
	49.30	52.32	−3.02	1.388
	47.27	40.70	6.57	−2.121
	37.62	36.88	0.74	−0.128
Schiller function	30.15	33.95	−3.80	1.424
	34.08	33.28	0.80	−0.196
	30.72	29.39	1.33	−0.432
	24.90	27.65	−2.75	0.974
	23.91	23.35	0.56	−0.241
	19.07	19.60	−0.53	0.093
	11.40	11.58	−0.18	−0.134
	8.63	7.87	0.76	−0.511
	5.74	6.17	−0.43	−0.116
	49.30	48.20	1.10	0.001
	47.27	40.23	7.04	−1.930
	37.62	37.23	0.39	0.063
	30.15	34.78	−4.63	1.564
	34.08	34.21	−0.13	0.179
One linear function	30.72	30.71	0.01	0.086
	24.90	29.07	−4.17	1.343
	23.91	24.78	−0.87	0.272
	19.07	20.76	−1.69	0.466
	11.40	11.22	0.18	−0.242
	8.63	6.31	2.32	−0.967
	5.74	3.96	1.78	−0.835

However, the mathematical functions that are used to characterize the relationship between capillary porosity and mechanical properties have a certain application prospect in the fields of well cementing. Further experimental research and statistical analysis will be processed in the following study.

3.5. SEM Findings

SEM images of the fracture surface morphologies of cement stone samples with w/c ratios of 0.40, 0.44, 0.50 at one day and seven days are shown in Figure 12. Image J was used to statistically analyze the morphologic characteristics of crystalline CH, 20 CH crystals.

In Figure 12, with the increase in the w/c ratio, the pore spaces of samples increased obviously, the side length of the formed CH crystals became larger and more regular. The proportion of large capillary pores increased correspondingly. When the w/c ratio is 0.40, only a few well-crystallized hexagonal and tabular CH crystals can be found, while the side length of the hexagonal CH crystals is mainly distributed in the range of 0.8~2.5 μm (Figure 12a). When the w/c ratio is 0.44, the formed CH crystals are in clusters, and most of them are well crystallized hexagonal and tabular, while the side length of the CH crystals is mainly distributed in the range of 1.3~3.6 μm (Figure 12b). When the w/c ratio is 0.50, compared to the samples with w/c ratios of 0.40 and 0.44, the formed CH crystals in Figure 11c are larger and looser, while the side length of the CH crystals is mainly distributed in the range of

1.9~5.3 μm (Figure 12c). Compared to the results in Figure 12c,d, it also can be found that the cement stone tends to be more compact as the hydration time increases.

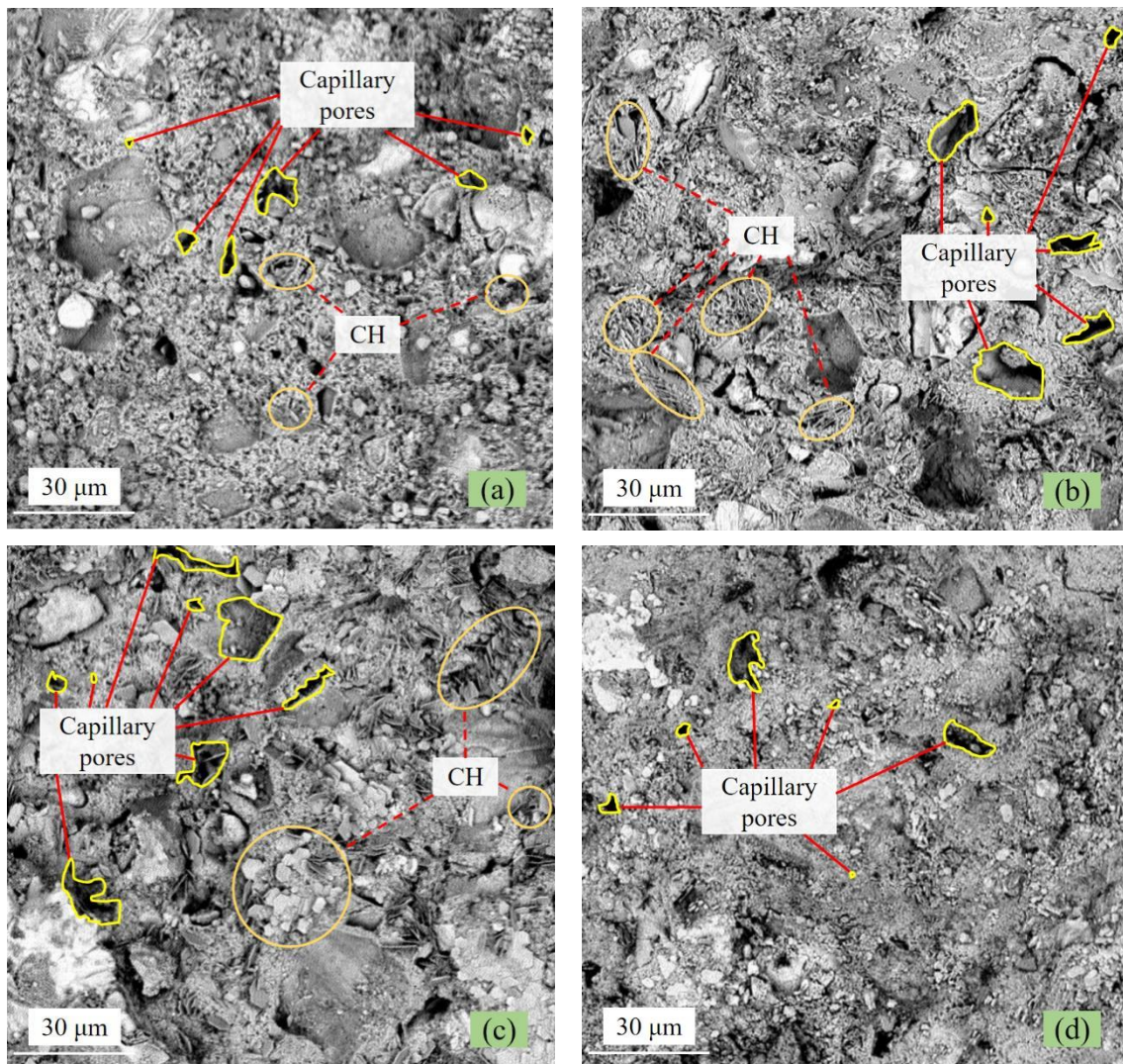


Figure 12. Microstructure of cement stone using SEM: (a) $w/c = 0.40$, 1 day; (b) $w/c = 0.44$, 1 day; (c) $w/c = 0.50$, 1 day; (d) $w/c = 0.50$, 7 days.

The cement particles in the cement slurry with a high w/c ratio have a relatively higher hydration degree compared to the cement stone with a low w/c ratio. However, the proportion of cement decreases as the w/c ratio increases, and the amount of hydration products decreases correspondingly (Figure 8, Figure 9, and Figure 12). Macroscopically, the mechanical properties of the cement stone decrease with the increase in the w/c ratio (Figure 6).

4. Conclusions

1. The simulated compressive strength and capillary porosity using the cement slurry hydration kinetics model established on HYMOSTRUC3D demonstrated a good agreement with the experimentally measured data, where the relative errors between the simulated results and measured results are within 0.6%~10.7% and 13.04~25.31% respectively.
2. With the increase in the w/c ratio, the volume content of hydration products and the compressive strength decreases, while the volume of pores and capillary porosity increases.

3. The compressive strength of cement stone is negatively correlated with capillary porosity. Capillary porosity is the main factor affecting the compressive strength of cement stone. In the well cementing industry, a lower w/c ratio should be selected as far as possible to prepare cement slurry and thus improve the early mechanical properties of the cement sheath.
4. The mathematical relationship between the measured capillary porosity and compressive strength of cement slurry is well fitted by the Balshin function ($R^2 = 0.95$), Ryshkewitch function ($R^2 = 0.94$), Schiller function ($R^2 = 0.96$), and the linear function ($R^2 = 0.95$). Those mathematical functions can be used to characterize and predict the quantitative relationship between the compressive strength and capillary porosity of cement stone. Those findings have a certain application prospect in the fields of well cementing, meanwhile, it can help to improve the accuracy of the model established on HYMOSTRUC3D.
5. The effects of the w/c ratio should be considered in building a broader mathematical function of the w/c ratio, porosity, and compressive strength.

Author Contributions: Conceptualization, S.Z. and T.L.; methodology, S.Z. and G.J.; software, S.Z. and P.G.; validation, S.Z., T.L., L.L., and P.G.; investigation, S.Z. and T.L.; resources, Y.F.; data curation, S.Z.; writing—original draft preparation, S.Z. and T.L.; writing—review and editing, S.Z., T.L., C.F., and B.Q.; visualization, S.Z. and L.L.; supervision, T.L.; project administration, T.L. and G.J. All authors have read and agreed to the published version of the manuscript.

Funding: This work was financially supported by the National Key Research and Development Program of China [Grant No. 2016YFE0204300], the National Natural Science Foundation of China [Grant No. 42072343].

Institutional Review Board Statement: Not applicable.

Informed Consent Statement: Not applicable.

Data Availability Statement: The data presented in this study are available on request from the corresponding author.

Acknowledgments: The authors thank the anonymous reviewers for their constructive comments, the editor for handling the paper, and the authors of their references.

Conflicts of Interest: The authors declare no conflict of interest.

References

1. Liu, C.J.; Huang, B.Z.; Xu, T.T. *Cement Injection Theory and Application in Oil and Gas Wells*; Petroleum Industry Press: Beijing, China, 2001.
2. Kremieniewski, M. Recipe of lightweight slurry with high early strength of the resultant cement sheath. *Energies* **2020**, *13*, 1583. [[CrossRef](#)]
3. Tang, J.; Zhang, C.; Zhang, B.; Fangfang, S.H.I. Cement bond quality evaluation based on acoustic variable density logging. *Pet. Explor. Dev.* **2016**, *43*, 514–521. [[CrossRef](#)]
4. Brandão, N.B.; Roehl, D.; de Andrade Silva, F.; e Silva, R.R. The impact of cement slurry aging creep on the construction process of oil wells. *J. Pet. Sci. Eng.* **2017**, *157*, 422–429. [[CrossRef](#)]
5. Li, M.; Deng, S.; Yu, Y.; Jin, J.; Yang, Y.; Guo, X. Mechanical properties and microstructure of oil well cement stone enhanced with Tetra-needle like ZnO whiskers. *Constr. Build. Mater.* **2017**, *135*, 59–67. [[CrossRef](#)]
6. Saleh, F.K.; Teodoriu, C.; Sondergeld, C.H. Investigation of the Effect of Cement Mixing Energy on Cement Strength and Porosity using NMR and UPV methods. *J. Nat. Gas Sci. Eng.* **2019**, *70*, 102972. [[CrossRef](#)]
7. Mohamadian, N.; Ramhormozi, M.Z.; Wood, D.A.; Ashena, R. Reinforcement of oil and gas wellbore cements with a methyl methacrylate/carbon-nanotube polymer nanocomposite additive. *Cem. Concr. Com.* **2020**, *114*, 103763. [[CrossRef](#)]
8. Visschedijk, A.J.; Denier van der Gon, H.A. Methane and ethane emission scenarios for potential shale gas production in Europe. *Adv. Geosci.* **2018**, *45*, 125–131. [[CrossRef](#)]
9. Cleland, K.D.J. Assessment of the durability of concrete from its permeation properties: A review. *Constr. Build. Mater.* **2001**, *15*, 93–103.
10. Schulze, J. Influence of water-cement ratio and cement content on the properties of polymer-modified mortars. *Cem. Concr. Res.* **1999**, *29*, 909–915. [[CrossRef](#)]

11. Rao, G.A. Role of water–binder ratio on the strength development in mortars incorporated with silica fume. *Cem. Concr. Res.* **2001**, *31*, 443–447. [[CrossRef](#)]
12. Rahmani, K.; Rahmanzadeh, B.; Piroti, S. Experimental study of the effect of water-cement ratio on compressive strength, abrasion resistance, porosity and permeability of nano silica concrete. *Frat. Ed. Integrità Strutt.* **2018**, *12*, 16–24. [[CrossRef](#)]
13. Li, L.; Zhang, H.; Guo, X.; Zhou, X.; Lu, L.; Chen, M.; Cheng, X. Pore structure evolution and strength development of hardened cement paste with super low water-to-cement ratios. *Constr. Build. Mater.* **2019**, *227*, 117108. [[CrossRef](#)]
14. Odler, I.; Robler, M. Investigations on the relationship between porosity, structure and strength of hydrated Portland cement pastes. II. Effect of pore structure and of degree of hydration. *Cem. Concr. Res.* **1985**, *15*, 401–410. [[CrossRef](#)]
15. Odler, I.; Abdul-Maula, S. Investigations on the relationship between porosity structure and strength of hydrated portland cement pastes III. Effect of clinker composition and gypsum addition. *Cem. Concr. Res.* **1987**, *17*, 22–30. [[CrossRef](#)]
16. Li, Y.X.; Chen, Y.M.; Wei, J.X.; He, X.Y.; Zhang, H.T.; Zhang, W.S. A study on the relationship between porosity of the cement paste with mineral additives and compressive strength of mortar based on this paste. *Cem. Concr. Res.* **2006**, *36*, 1740–1743. [[CrossRef](#)]
17. Ozturk, A.U.; Baradan, B. A comparison study of porosity and compressive strength mathematical models with image analysis. *Comput. Mater. Sci.* **2008**, *43*, 974–979. [[CrossRef](#)]
18. Ibrahim, A.; Mahmoud, E.; Yamin, M.; Patibandla, V.C. Experimental study on Portland cement pervious concrete mechanical and hydrological properties. *Constr. Build. Mater.* **2014**, *50*, 524–529. [[CrossRef](#)]
19. Anya, A.; Emadi, H.; Watson, M. An empirical model for calculating uniaxial compressive strength of oil well cements from ultrasonic pulse transit time measurements. *J. Pet. Sci. Eng.* **2019**, *183*, 106387. [[CrossRef](#)]
20. Wei, T.C.; Cheng, X.W.; Wang, S.Z.; Lin, L.; Long, D.; Guo, X.Y. Study on pore volume fractal dimension of microsphere low density cement and its relationship with pore structure and mechanical properties. *Mater. Rep.* **2016**, *30*, 415–419.
21. Loenzoni, R.; Paciornik, S.; Silva, F.A. Characterization by microcomputed tomography of class G oil well cement paste exposed to elevated temperatures. *J. Pet. Sci. Eng.* **2019**, *175*, 896–904. [[CrossRef](#)]
22. Lu, S.; Landis, E.N.; Keane, D.T. X-ray microtomographic studies of pore structure and permeability in Portland cement concrete. *Mater. Struct.* **2006**, *39*, 611–620. [[CrossRef](#)]
23. Erdoğan, S.T.; Nie, X.; Stutzman, P.E.; Garboczi, E.J. Micrometer-scale 3D shape characterization of eight cements: Particle shape and cement chemistry, and the effect of particle shape on laser diffraction particle size measurement. *Cem. Concr. Res.* **2010**, *40*, 731–739. [[CrossRef](#)]
24. Cepuritis, R.; Garboczi, E.J.; Ferraris, C.F.; Jacobsen, S.; Sørensen, B.E. Measurement of particle size distribution and specific surface area for crushed concrete aggregate fines. *Adv. Powder Technol.* **2017**, *28*, 706–720. [[CrossRef](#)]
25. Ueda, T.; Oki, T.; Koyanaka, S. Experimental analysis of mineral liberation and stereological bias based on X-ray computed tomography and artificial binary particles. *Adv. Powder Technol. Int. J. Soc. Powder Technol.* **2018**, *29*, 462–470. [[CrossRef](#)]
26. Nitka, M.; Tejchman, J. A three-dimensional meso-scale approach to concrete fracture based on combined DEM with X-ray CT images. *Cem. Concr. Res.* **2018**, *107*, 11–29. [[CrossRef](#)]
27. Gallucci, E.; Scrivener, K.; Groso, A.; Stampanoni, M.; Margaritondo, G. 3D experimental investigation of the microstructure of cement pastes using synchrotron X-ray microtomography (μ CT). *Cem. Concr. Res.* **2007**, *37*, 360–368. [[CrossRef](#)]
28. Bossa, N.; Chaurand, P.; Vicente, J.; Borschneck, D.; Levard, C.; Aguerre-Chariol, O.; Rose, J. Micro- and nano-X-ray computed-tomography: A step forward in the characterization of the pore network of a leached cement paste. *Cem. Concr. Res.* **2015**, *67*, 138–147. [[CrossRef](#)]
29. Yang, X.; Kuru, E.; Gingras, M.; Iremonger, S. CT-CFD integrated investigation into porosity and permeability of neat early-age well cement at downhole condition. *Constr. Build. Mater.* **2019**, *205*, 73–86. [[CrossRef](#)]
30. Jennings, H.M.; Johnson, S.K. Simulation of microstructure development during the hydration of a cement compound. *J. Am. Ceram. Soc.* **1986**, *69*, 790–795. [[CrossRef](#)]
31. Van Breugel, K. Numerical simulation of hydration and microstructural development in hardening cement-based materials. *Cem. Concr. Res.* **1992**, *25*, 319–331. [[CrossRef](#)]
32. Ye, G. Experimental Study and Numerical Simulation of the Development of the Microstructure and Permeability of Cementitious Materials. Ph.D. Thesis, Delft University of Technology, Delft, The Netherland, 2003.
33. Gao, P. Simulation of Hydration and Microstructure Development of Blended Cements. Ph.D. Thesis, Delft University of Technology, Delft, The Netherlands, 2018.
34. Navi, P.; Pignat, C. Simulation of cement hydration and the connectivity of the capillary pore space. *Adv. Cem. Based Mater.* **1996**, *4*, 58–67. [[CrossRef](#)]
35. Bentz, D.P. Three-dimensional computer simulation of Portland cement hydration and microstructure development. *J. Am. Ceram. Soc.* **1997**, *80*, 3–21. [[CrossRef](#)]
36. Maekawa, K.; Ishida, T.; Kishi, T. Multi-scale modeling of concrete performance. *J. Adv. Concr. Technol.* **2003**, *1*, 91–126. [[CrossRef](#)]
37. Bishnoi, S.; Scrivener, K.L. μ ic: A new platform for modelling the hydration of cements. *Cem. Concr. Res.* **2009**, *39*, 266–274. [[CrossRef](#)]
38. Bullard, J.W. A three-dimensional microstructural model of reactions and transport in aqueous mineral systems. *Model. Simul. Mater. Sci. Eng.* **2007**, *15*, 711–738. [[CrossRef](#)]
39. Bullard, J.W.; Lothenbach, B.; Stutzman, P.E.; Snyder, K.A. Coupling thermodynamic and digital image models to simulate hydration and microstructure development of Portland cement pastes. *J. Mater. Res.* **2011**, *26*, 609–622. [[CrossRef](#)]

40. Park, K.B.; Noguchi, T.; Plawsky, J. Modeling of hydration reactions using neural networks to predict the average properties of cement paste. *Cem. Concr. Res.* **2005**, *35*, 1676–1684. [[CrossRef](#)]
41. Lothenbach, B.; Maciej, Z. Application of thermodynamic modelling to hydrated cements. *Cem. Concr. Res.* **2019**, *123*, 105779. [[CrossRef](#)]
42. Koenders, E.A.B. Simulation of Volume Changes in Hardening Cement-Based Materials. Ph.D. Thesis, Delft University of Technology, Delft, The Netherlands, 1997.
43. Ye, G.; Lura, P.; Breugel, K.V. Modelling of water permeability in cementitious materials. *Mater. Struct.* **2006**, *39*, 877–885. [[CrossRef](#)]
44. Qian, Z.; Schlangen, E.; Ye, G.; Van Breugel, K. Prediction of mechanical properties of cement paste at microscale. *Mater. Constr.* **2010**, *60*, 7–18. [[CrossRef](#)]
45. Pandey, S.P.; Sharma, R.L. The influence of mineral additives on the strength and porosity of OPC mortar. *Cem. Concr. Res.* **2000**, *30*, 19–23. [[CrossRef](#)]
46. Kearsley, E.P.; Wainwright, P.J. The effect of porosity on the strength of foamed concrete. *Cem. Concr. Res.* **2002**, *32*, 233–239. [[CrossRef](#)]
47. Sun, Z.; Ye, G.; Shah, S.P. Microstructure and Early-Age Properties of Portland Cement Paste—Effects of Connectivity of Solid Phases. *ACI Mater. J.* **2005**, *102*, 122–129.
48. Ouyang, X.; Gao, P.; Ye, G.; van Breugel, K. Effect of Filler-Hydrates Adhesion Properties on Cement Paste Strength. *ACI Mater. J.* **2018**, *115*, 437–447. [[CrossRef](#)]
49. Bird, M.B.; Butler, S.L.; Hawkes, C.D.; Kotzer, T. Numerical modeling of fluid and electrical currents through geometries based on synchrotron X-ray tomographic images of reservoir rocks using Avizo and COMSOL. *Comput. Geosci* **2014**, *73*, 6–16. [[CrossRef](#)]
50. Fan, N.; Wang, J.; Deng, C.; Fan, Y.; Wang, T.; Guo, X. Quantitative characterization of coal microstructure and visualization seepage of macropores using CT-based 3D reconstruction. *J. Nat. Gas Sci. Eng.* **2020**, *81*, 103384. [[CrossRef](#)]
51. Fusses, F.; Xiao, X.; Schrank, C.; De Carlo, F. A brief guide to synchrotron radiation-based microtomography in (structural) geology and rock mechanics. *J. Struct. Geol.* **2014**, *65*, 1–16. [[CrossRef](#)]
52. Liu, K.; Cheng, X.; Ma, Y.; Gao, X.; Yu, Y.; Zhang, C.; Guo, X.; Zhuang, J. Visualization and quantification of pore structure of oil-well cement slurry in liquid-solid transition stage using high-resolution computed tomography. *Cem. Concr. Compos.* **2020**, *111*, 103633. [[CrossRef](#)]
53. Yio, M.H.N.; Wong, H.S.; Buenfeld, N.R. Representative elementary volume (REV) of cementitious materials from three-dimensional pore structure analysis. *Cem. Concr. Res.* **2017**, *102*, 187–202. [[CrossRef](#)]
54. Wildenschild, D.; Sheppard, A.P. X-ray imaging and analysis techniques for quantifying pore-scale structure and processes in subsurface porous medium systems. *Adv. Water Resour.* **2013**, *51*, 217–246. [[CrossRef](#)]
55. Wang, X.Y.; Lee, H.S. Modeling of hydration kinetics in cement-based materials considering the effects of curing temperature and applied pressure. *Constr. Build. Mater.* **2012**, *28*, 1–13. [[CrossRef](#)]
56. Nguyen, V.T. Rice Husk Ash as a Mineral Admixture for Ultra-High-Performance Concrete. Ph.D. Thesis, Delft University of Technology, Delft, The Netherlands, 2011.
57. Jin, X.; Wang, Y.; Tian, Y.; Jin, N. Research on kinetics model of cement hydration based on microstructure information. *J. Build. Mater.* **2014**, *17*, 862–867.
58. Zhang, M.Z.; Ye, G.; van Breugel, K. A numerical-statistical approach to determining the representative elementary volume (REV) of cement paste for measuring diffusivity. *Mater. De Constr.* **2010**, *60*, 7–20. [[CrossRef](#)]
59. Silva, D.A.; John, V.M.; Ribeiro, J.L.D.; Roman, H.R. Pore size distribution of hydrated cement pastes modified with polymers. *Cem. Concr. Res.* **2001**, *31*, 1177–1184. [[CrossRef](#)]
60. Lu, S.C.; Wang, X.Y.; Meng, Z.R.; Deng, Q.; Peng, F.; Yu, C.; Hu, X.; Zhao, Y.; Ke, Y.; Qi, F. The mechanical properties, microstructures and mechanism of carbon nanotube-reinforced oil well cement-based nanocomposites. *RSC Adv.* **2019**, *9*, 26691–26702. [[CrossRef](#)]
61. Wu, D.J.; She, W.; Miao, C.W.; Yang, Y. Simulation of cement hydration microstructure evolution process based on improved CEMHYD3D model. *J. Build. Mater.* **2020**, *23*, 11–17.
62. Taylor, H.F.W. *Cement Chemistry*, 2nd ed.; Thomas Telford: Telford, UK, 1997.
63. Mindess, S.; Darwin, D.; Young, J.F. *Concrete*; Prentice Hall: Englewood Cliffs, NJ, USA, 2003.